

Becoming Stable and Strong: The Interplay Between Vinculin Exchange Dynamics and Adhesion Strength During Adhesion Site Maturation

Christoph Möhl,¹ Norbert Kirchgeßner,¹ Claudia Schäfer,¹ Kevin Küpper,¹ Simone Born,¹ Gerold Diez,² Wolfgang H. Goldmann,² Rudolf Merkel,¹ and Bernd Hoffmann^{1*}

¹*Institute of Bio- and Nanosystems, IBN-4, Biomechanics, Research Centre Jülich GmbH, Jülich, Germany*

²*Center for Medical Physics and Technology, Biophysics Group, Friedrich-Alexander-University of Erlangen-Nuremberg, Erlangen, Germany*

The coordinated formation and release of focal adhesions is necessary for cell attachment and migration. According to current models, these processes are caused by temporal variations in protein composition. Protein incorporation into focal adhesions is believed to be controlled by phosphorylation. Here, we tested the exchange dynamics of GFP-vinculin as marker protein of focal adhesions using the method of Fluorescence Recovery After Photobleaching. The relevance of the phosphorylation state of the protein, the age of focal adhesions and the acting force were investigated. For stable focal adhesions of stationary keratinocytes, we determined an exchangeable vinculin fraction of 52% and a recovery half-time of 57 s. Nascent focal adhesions of moving cells contained a fraction of exchanging vinculin of 70% with a recovery half-time of 36 s. Upon maturation, mean saturation values and recovery half-times decreased to levels of 49% and 42 s, respectively. Additionally, the fraction of stably incorporated vinculin increased with cell forces and decreased with vinculin phosphorylation within these sites. Experiments on a nonphosphorylatable vinculin mutant construct at phosphorylation site tyr1065 confirmed the direct interplay between phosphorylation and exchange dynamics of adhesion proteins during adhesion site maturation. *Cell Motil. Cytoskeleton* 66: 350–364, 2009. © 2009 Wiley-Liss, Inc.

Key words: vinculin; FRAP; exchange dynamics; focal adhesion; cell force; tyrosine phosphorylation

INTRODUCTION

Cell adhesion and migration are two vital processes that are fully dependent on a controlled adhesion mechanism. Migrating cells feature structural polarity with obvious differences between front and rear and pronounced adhesion dynamics with coordinated formation and release of focal adhesion sites (FAs). New adhesion sites mechanically couple the actin network to extracellular matrix proteins at the cell front. Simultaneously, adhesion sites located at the rear of moving cells are dissolved while myosin-driven contraction of actin moves the cell body forward [Lauffenburger and Horwitz,

Additional Supporting Information may be found in the online version of this article.

Contract grant sponsors: BFHZ, BaCaTec, and DAAD.

*Correspondence to: Bernd Hoffmann, Institute of Bio- and Nanosystems, IBN-4, Research Centre Jülich GmbH, Jülich 52425, Germany. E-mail: b.hoffmann@fz-juelich.de

Received 24 November 2008; Revised 6 April 2009; Accepted 8 April 2009

Published online 6 May 2009 in Wiley InterScience (www.interscience.wiley.com). DOI: 10.1002/cm.20375

1996]. This mechanism implies several regulatory events which result in an adhesion site maturation process [Rottner et al., 1999].

Adhesion sites are complex, dynamic structures composed of more than 50 different proteins [Zamir and Geiger, 2001; Zaidel-Bar et al., 2007a]. In locomoting cells, new adhesions known as focal complexes (FXs) develop near the leading edge by clustering of integrins at distinct spots. These integrins are bound to extracellular matrix molecules including fibronectin, laminin or collagen [Zaidel-Bar et al., 2003]. Within the cell, integrins are indirectly coupled to actin filaments through adaptor proteins like vinculin or talin [Petit and Thiery, 2000]. While many FXs disappear during incomplete adhesion of lamellipodia, some of them grow and develop into nascent FAs. This process goes along with the incorporation of adaptor proteins like zyxin or α -actinin and regulatory kinases like focal adhesion kinase (FAK). As the cell moves forward, FAs remain relatively stable with respect to the substrate and develop over time into mature FAs. Thus, during maturation FAs come closer to the trailing edge of the cell, where they finally dissolve [Webb et al., 2002; Zaidel-Bar et al., 2004]. In nonmigrating cells, the assembly and disassembly of new FAs is strongly reduced, resulting in a much longer lifetime of FAs. Here, FAs can even develop further to fibrillar adhesions which are highly elongated, stable structures. This process goes along with changes in protein composition; the reduced protein level of vinculin is an example for that [Zamir et al., 1999]. An additional process involved in FA maturation is protein modification. This takes place mainly at the level of protein phosphorylation. Kinases like FAK or cellular sarcoma kinase, c-src are well characterized tyrosine kinases which phosphorylate several proteins specific to FAs such as vinculin or paxillin [Thomas et al., 1999; Zhang et al., 2004]. For vinculin, these phosphorylation events are believed to be stabilizing an open conformation. Moreover, this open conformation possibly exhibits enhanced binding affinities to other molecules of young FA and could contribute to high tyrosine phosphorylation levels in young FAs [Zhang et al., 2004]. The phosphorylation levels decrease again upon FA aging [Zamir et al., 1999; Zaidel-Bar et al., 2007b]. Vinculin is structurally made up of a globular head linked to the tail domain by a proline-rich region. Interaction sites for numerous binding partners on vinculin have been mapped. In the closed or inactive state of vinculin, all binding as well as phosphorylation sites seem to be masked by the intramolecular interaction between the head and tail domain [Zhang et al., 2004; Ziegler et al., 2006]. Upon activation, the head and tail domain disengage thus exposing ligand-binding sites. However, the mechanism for vinculin activation remains unclear. It was demonstrated by FRET

experiments that talin together with actin has the ability to displace the head from the tail [Chen et al., 2005]. Similar abilities have been reported for phospholipids such as PIP2 [Johnson and Craig, 1995; Gilmore and Burridge 1996]. Furthermore, vinculin phosphorylation at Y100 and Y1065 [Zhang et al., 2004] as well as Y822 [Subauste et al., 2004] have been shown to play an important role in vinculin activation, stabilization and ligand binding.

Functionally, FAs are strongly connected with cellular force transduction. For adherent cells, force transmission occurs exclusively at adhesion sites [Balaban et al., 2001; Beningo et al., 2001]. Moreover, inhibition of force generation results in loss of adhesion sites and apoptosis [Volberg et al., 1994; Chrzanoska-Wodnicka and Burridge, 1996; Grinnell et al., 1999; Wang et al., 2000]. Traction force measurements of migrating fibroblasts and fish keratocytes revealed force concentration at the tail end [Galbraith and Sheetz 1997; Oliver et al., 1999]. These data led to suggestions of a mainly tensile stress-dependent detachment of FAs at the rear end [Galbraith and Sheetz 1997; Kirfel et al., 2004]. Furthermore, rear adhesion sites are typically larger [Anderson and Cross, 2000]. Also for sessile cells, a correlation between force magnitude and size of adhesions has been found [Balaban et al., 2001; Bershadsky et al., 2003]. Several adhesion models take this correlation into consideration [Geiger and Bershadsky, 2002; Vogel and Sheetz, 2006]. Moreover, FA size adaptations have been found upon applying cellular adhesion strength or external force fields [Riveline et al., 2001]. Interestingly, these adaptations are only detectable for very young FAs while older FAs do barely respond to size changes of internal or external signals [Galbraith et al., 2002]. The reason for this loss of responsiveness is unsolved but might be related to changes in protein composition or phosphorylation upon FA maturation.

Most FA molecules are soluble proteins which are incorporated into FAs by specific binding. These molecules undergo a permanent exchange process between bound and unbound states. Most likely, they exhibit several bound states differing in number and/or strength of specific bonds to other parts of FAs. Changes in size of young FAs can occur only when the average exchange rates of FA molecules are altered. Recent studies have analyzed exchange dynamics of several FA proteins such as paxillin or vinculin in stationary cells by FRAP (Fluorescence recovery after photobleaching) [Lele et al., 2006; Cohen et al., 2006; Lele et al., 2008]. Using this technique, the very slowly exchanging molecular states give rise to a “not exchanging fraction” while the exchange rate of the other molecules is characterized by the half-time of recovery. The aforementioned FRAP analyses revealed surprisingly high exchanging fractions

for both proteins of $\sim 50\%$ and recovery halftimes in the range of 15–80 s. Furthermore, identical analyses on cells with blocked tyrosine dephosphorylation by mutated SH2-containing protein tyrosine phosphatase 2 (Shp2) indicate a correlation between phosphorylation and exchange dynamics with strongly increased recovery rates for both proteins. Enhanced rates can be rescued to wild-type levels by inhibition of FAK [von Wichert et al., 2003].

In order to characterize the connection between force, phosphorylation, FA maturation state and protein exchange dynamics, we performed FRAP analyses on motile and sessile keratinocytes transfected with GFP-vinculin. We found that the degree of vinculin exchange is strongly increased in nascent FAs of motile cells and decreases during the lifetime of FAs. The lowest exchanging fraction of vinculin and the slowest recovery were found in FAs of sessile cells. Moreover, we determined vinculin phosphorylation levels at tyrosine 1065. In all analyses, vinculin exchange dynamics in FAs was correlated with vinculin phosphorylation levels. Mutating tyr1065 to phenylalanine (Y1065F) abolished phosphorylation at that site and equalized exchange dynamics of nascent and mature FAs in direction of reduced dynamics. In addition, traction force measurements revealed a strong correlation between low tyrosine phosphorylation levels, reduced protein exchange dynamics and enhanced force application.

MATERIALS AND METHODS

Cell Culture

Normal human epidermal keratinocytes (NHEK) from neonatal foreskin were purchased from Lonza (Verviers, Belgium). Subcultures were grown at 37°C and 5% CO_2 in complete keratinocyte basal medium (KGM, Lonza). Cells were harvested for subculturing or subsequent experiments using 0.025% Trypsin and 0.01% EDTA in Hank's buffered salt solution (HBSS, Lonza). They were used for not more than four passages. For all experiments, 30,000–50,000 cells were plated either on self made glass bottom petri dishes (thickness of glass bottom: $170\ \mu\text{m}$) or on PDMS elastomer coated cover slips (see below). For immunofluorescence assays, glass cover slips were placed in 12-well-dishes. All glass surfaces were coated with $2.5\ \mu\text{g}/\text{cm}^2$ human plasma fibronectin (BD Biosciences, San Jose, CA) for 30 min at RT before use. PDMS substrates were coated with $5\ \mu\text{g}/\text{cm}^2$ human plasma fibronectin for 2 h at 37°C . Homogeneity of coating of PDMS substrates was analyzed using rhodamine-labeled fibronectin (Cytoskeleton, Denver, CO) at identical concentrations and coating conditions as given above. In some experiments, keratinocytes were

treated with 50 nM human epidermal growth factor (EGF, Sigma, St. Louis, MO) which was added 1 h before analysis to induce cell migration. For experiments with stationary cells, cultures were grown until they reached $\sim 75\%$ confluency while migrating cells were observed at lower densities of not more than 20% confluency. Here, only solitary cells, exhibiting a polarized morphology with a lamella extended in the direction of migration, were selected for measurements.

Plasmid Constructs and Transfection

In order to inhibit vinculin phosphorylation at tyrosine (Y) 1065, a PCR site-directed mutagenesis was performed exchanging nucleotides TAC encoding tyrosine 1065 against TTC encoding phenylalanine (F). *EGFP-vinculin Y1065F* open reading frame was ligated into plasmid pcDNA3.1/Hygro (Invitrogen, Karlsruhe, Germany) resulting in plasmid EGFP-vinculinY1065F. Transient transfections of keratinocytes with EGFP-vinculin (provided by B. Geiger, Weizmann Institute of Science, Rehovot, Israel) and EGFP-vinculinY1065F were performed with Transit Keratinocyte reagent (Mirus, Madison, WI, USA) according to the manufacturer's instructions.

Preparation and Characterization of Elastomeric Substrates

Elastomeric substrates were made of polydimethylsiloxane (PDMS, Sylgard 184, Dow Corning GmbH, Wiesbaden, Germany). Substrates were made and characterized as described earlier [Cesa et al., 2007]. Briefly, Sylgard was mixed in a 55 to 1 (base to cross-linker, by weight) ratio and $80\ \mu\text{m}$ thick substrates were created using spacers of defined thickness for sandwich formation. After curing over night at 60°C , cross-linked PDMS substrates exhibited a Young's modulus of 11 kPa and a Poisson's ratio of 0.5. The used PDMS-oils were all from the same batch. Calibration experiments were performed using cross-linked PDMS rods. Rods were stretched and released in repetitive and defined steps. Applied forces as well as the diameter of each rod were permanently measured [Cesa et al., 2007] and allowed the accurate determination of Young's modulus and Poisson ratio. Substrate parameters were determined several times from independent cross-linking reactions and no changes could be observed. This argues for a high reproducibility of used PDMS substrates. For preparation of elastic substrates with fluorescent beads on their surface, $0.2\ \mu\text{m}$ Crimson-FluoSpheres (Invitrogen) (5%) were homogenized in still fluid PDMS [Merkel et al., 2007]. Bead-labeled PDMS was coated over a silicon dioxide surface silanized with trichloro (1H,1H,2H,2H-perfluorooctyl)silane (Sigma). Surfaces

were either flat or microstructured (2- μm dots arranged in a square lattice of 3.5 μm lattice constant). The layer thickness was reduced to less than 0.5 μm by vigorously wiping with optical paper. Subsequently, the bead labeled PDMS layer was overlaid with unlabeled PDMS to a final thickness of 100 μm and cross-linked as described above.

Microscopic Techniques

For cell force analyses, living cells were analyzed using a Zeiss Axiovert 200 inverted microscope (Cell Observer, Carl Zeiss MicroImaging GmbH, Jena, Germany). Live cell imaging was performed by phase contrast as well as by fluorescence microscopy with filter sets appropriate for GFP visualization using a 40 \times , 1.3 NA, PlanNeofluar oil objective (Carl Zeiss). Image acquisition was performed using a CCD camera (Axiocam MRM, Carl Zeiss). Time-lapse movies for mean substrate deformation measurements were recorded under live cell conditions using either a confocal microscope (LSM510Meta; Zeiss) or the Cell Observer HS live cell imaging system (Carl Zeiss) with an EM CCD camera (model C9100-02, Hamamatsu Photonics, Hamamatsu, Japan). Images were taken with a 40 \times , 1.3 NA, PlanNeofluar PH3 oil objective (Carl Zeiss). To study cells and fluorescent beads simultaneously, samples were imaged in two channels by alternating phase contrast and fluorescence microscopy for 58 to 120 min at a frame rate of 20 s per channel.

FRAP experiments were performed on the LSM510Meta confocal microscope with a 63 \times , 1.4 NA, PlanApochromat oil objective (Carl Zeiss). All microscopes used for live cell analysis were equipped with incubators to maintain cells at 37°C and 5% CO₂.

Immunofluorescence images of fixed cells were performed using the confocal microscope. For immunofluorescence analyses, the 488 nm line of an argon-ion laser and the 543 nm helium-neon laser were used together with appropriate filter sets for simultaneous detection of green (Cy2) and red (Cy3) fluorescent light.

Image analyses were performed with MATLAB (The Mathworks, version 7.6, Natick, MA). Automated detection of focal adhesions by the “water” algorithm and determination of intensity ratio (phospho-vinculin divided by total vinculin), FA area and center of mass localization were performed as described by [Zamir et al., 1999] using the following parameter values: filter box size, 15 \times 15 μm^2 ; minimum patch area ($A_{\text{min}}^{\text{p}}$), 0.5 μm^2 ; critical patch size for merging ($A_{\text{min}}^{\text{m}}$), 0.56 μm^2 . The leading edge was marked manually to calculate its distance from FAs. This quantity was defined as the shortest distance between the leading edge and the FA center of mass.

Immunofluorescence and Western Blot Analysis

Cells were cultured as described above and fixed with 3.7% formaldehyde (Merck, Darmstadt, Germany) in cytoskeleton buffer, (CB: 150 mM NaCl, 5 mM MgCl₂, 5 mM EGTA, 5 mM glucose, 10 mM 2-(*N*-morpholino)ethanesulfonic acid, pH 6.1) at 37°C for 20 min [Small, 1981]. For labeling against vinculin and actin, fixed cells were washed in CB, permeabilized with 0.2% Triton-X100, Sigma in CB for 10 min, rinsed with CB, and treated with blocking solution (5% skim milk powder + 0.2% Tween20 (Sigma) in CB) for 60 min. Samples were incubated with primary antibodies solubilized in blocking solution (1:100 dilution) for 45 min at 37°C. After washing three times with blocking solution for 5 min each, cells were incubated with 1:100 dilutions of secondary antibodies and for actin staining with 1:100 dilutions of Alexa Fluor488-Phalloidin (Molecular Probes, Eugene OR) in blocking solution for 45 min at 37°C. After washing with blocking solution, samples were rinsed with water and mounted on glass slides in Gel Mount (Biomed, Foster City, CA) with addition of 0.1% (w/v) 1,4-Diazabicyclooctane (Sigma). Simultaneous labeling of total vinculin and phosphorylated vinculin was performed as described above except that PBS buffer was used instead of CB. Additionally, blocking was performed with 10% goat serum (Sigma) in PBS. For comparison, all vinculin double staining experiments were performed at the same time. Microscopic analyses of all samples were done with identical image parameters. Primary antibodies used were against vinculin (monoclonal, clone HVIN-1, Sigma) and against phospho-vinculin (tyr1065, polyclonal, Chemicon, Hofheim, Germany). Cy2 goat anti rabbit and Cy3 goat anti mouse were used as secondary antibodies (Jackson Immuno Research, Suffolk, UK).

In order to determine expression levels of used GFP-vinculin constructs, Western blot analyses were performed. Cells were cultured in 6 cm cell culture dishes (Nunc) for 2 days at a density of 50–70% confluency and subsequently transfected with GFP-vinculin and GFP-vinculinY1065F, respectively. After additional 48 h the transfection efficiency was determined. Cells were then washed with cold PBS, and lysed in 250 μl of lysis-buffer (10 mM Tris, 158 mM NaCl, 1 mM EDTA, 0.1% SDS, 1% sodiumdeoxycholat, 1% Triton X-100, 1% protease inhibitor for mammalian cells, Sigma, 1% phosphatase inhibitor for mammalian cells, Sigma) per culture dish. After 30 min of incubation at 4°C lysed cells were harvested and centrifuged at 13,200 \times *g* for 15 min at 4°C. 20 μg of protein crude extracts were separated on a 6% SDS-polyacrylamide gel and subsequently analyzed by Western blotting. As control protein, crude extracts of untransfected keratinocytes as well as of a mouse embryonic fibroblast vinculin^{-/-} knock out cell

line were loaded. Protein contents were equalized using tubulin (β -tubulin, clone TUB 2.1, Sigma) as constitutively expressed standard. Subsequently, protein levels for vinculin (HVIN-1, Sigma) were determined. Secondary antibodies (Sigma) were coupled to alkaline phosphatase. Immune complexes were visualized with a BCIP/NBT-Blue Liquid Substrate System (Sigma). Quantification of Western blots was performed with the ImageJ software using the gel analyzing function of the program.

Data Evaluation

As shown in the results section, FRAP measurements on focal adhesions capture two species of vinculin molecules, namely the freely diffusing cytosolic fraction and the fraction residing at binding sites within FAs. The underlying theoretical considerations and mathematical equations for determining both fractions as well as for calculating recovery halftimes ($t_{1/2}$) and mean saturation values are given in the Supporting Information section.

Significance tests were performed as described by [Kesel et al., 1999]. In brief, all data were tested for normal distribution by the Kolmogoroff-Smirnow and the David test. Homogeneity of variances was tested by the F-test. Since all data were normally distributed but sometimes heterogeneous in variance, the Weir test ($P = 0.05$) was chosen to detect significant differences between individual normal distributions of small size.

FRAP-Analyses

GFP-labeled proteins were bleached using the 488 nm argon laser line of the confocal microscope (LSM510Meta, Carl Zeiss) at full intensity. During image acquisition, laser power was reduced to 0.1–0.25% to minimize undesired photobleaching. For internal control, FAs were always bleached simultaneously with cytoplasmic areas of identical size. Typical data are shown in Fig. 2. As described in the result section, fluorescence recovery in FAs consisted of an initial rapid recovery phase dominated by cytoplasmic diffusion and a second much slower recovery phase caused by binding kinetics. Both phases were analyzed separately.

For the analysis of the fast first phase, data were collected at a rate of 11 frames per second. To eliminate the background from the raw intensity $I(t)$, an offset I_{oi} was defined as the intensity at the first time point after bleaching ($t = 0$ s). The curves were normalized and corrected for background due to the following equation: $I_{ni}(t) = \frac{I(t) - I_{oi}}{I_{si} - I_{oi}}$, where I_{ni} is the normalized intensity and I_{si} the intensity at the end of the initial recovery phase at $t = 16$ s. Note, that the curves of the initial fast recovery phase were not corrected for photobleaching since the time period of examination was not more than 25 s.

To analyze the second, slower recovery phase, data were collected at a rate of one frame per 2 s. The curves were corrected for photobleaching as well as cytoplasmic background as follows: Since the cytoplasmic background of migrating cells sometimes changed with time, an offset $I_{off}(t)$ was subtracted from each raw recovery curve to eliminate background fluorescence emitted by GFP-tagged proteins in the cytoplasm and incomplete bleaching. The offset was calculated as follows:

$I_{off}(t) = I_{ad}(t_k) - (I_{cp}(t_k) - I_{cp}(t))$, with I_{ad} denoting the fluorescence intensity of the bleach field at the FA and I_{cp} denoting the fluorescence intensity of the bleach field at the cytoplasm. The time point t_k was manually selected, where a kink in the recovery curve was visible (Fig. 2). Subtraction of I_{off} set the intensity of the recovery curve at t_k to zero and thus eliminated the first recovery phase from the data. This allowed treating the resulting curves beyond t_k as exclusively protein exchange driven recoveries (see also results section). Background elimination, correction for unintended photobleaching and normalization to the prebleach intensity was performed due to the following equation:

$$I_n(t) = \frac{I_{ad}(t) - I_{off}(t)}{(I_{ref}(t) - I_{off}(t))I_0},$$

where $I_n(t)$ is the normalized and corrected intensity and $I_{ref}(t)$ is the mean intensity of focal adhesions that were not bleached. $I_{off}(t)$ and $I_{ad}(t)$ were defined above and the prebleach intensity I_0 was determined according to $I_0 = \langle \frac{I_{ad}(t) - I_{off}(t)}{I_{ref}(t) - I_{off}(t)} \rangle$, where the angle brackets signify the average of the last 10 data points before bleaching.

The saturation value I_{sat} was calculated as the mean intensity of all points between 290 and 300 s after photobleaching. As diffusion in the cytoplasm was removed from the processed data, recovery could be described by a single kinetic model according to Eq. 3 (see Supporting Information). The solution (Eq. 5, see Supporting Information) was fitted to $\frac{I_n(t)}{I_{sat}}$ using the MATLAB function `fminsearch` (The Mathworks) to calculate the recovery half-time, $t_{1/2}$.

Traction Measurements and Force Calculation

Keratinocytes were grown on elastic PDMS substrates with embedded microbeads for one day and were induced for migration as described above. Time-lapse movies were recorded and image analysis was performed using MATLAB (The Mathworks) as software. Manual tracking of cell positions over time was performed with ImageJ (Wayne Rasband, U. S. National Institutes of Health) using the point tool.

Bead displacements were extracted automatically from the fluorescence micrograph time series. In the first

image, bead positions were determined by cross-correlation with a randomly chosen bead as template. In all later images, cross-correlation analyses for each detected bead were performed using the first image of the respective bead as template. Sample drift correction and correction for erroneously assigned beads were performed as previously described [Merkel et al., 2007]. This procedure yielded bead positions to an accuracy of ~ 10 nm. Bead displacements were calculated by subtracting bead positions of each frame from bead positions of a reference image without substrate deformation. The duration of time series was chosen long enough that either the first or the last image of a time series showed the cell well outside the analyzed area. The respective image was used as reference.

Mean substrate deformations over 30 min were quantified by transferring bead displacements of each frame to a cell-fixed coordinate system with its origin in the nucleus center and the y-axis pointing in the direction of migration. As the cell was constantly moving, the cell coordinate system had to be shifted and rotated for every frame (see Supporting Information, Fig. S1). The position of the nucleus center was determined by calculating the mean of four edge coordinates of the nucleus manually tracked over time. The cell orientation was determined from the bright halo present in phase contrast microscopy at the cell's rear end. The orientation was calculated for every time step with two manually defined points on the halo. To obtain a smooth motion of the cell coordinate system, all manually tracked coordinates were averaged over 30 time steps. Automatically detected bead positions were not averaged over time. To calculate mean bead displacements over time, rotated images were subdivided in squares with an edge length of $3.6 \mu\text{m}$. The bead displacement for each square was calculated by the mean of the displacement vectors from the beads located in the corresponding square at every time step.

For cell force analyses, substrate deformations of GFP-vinculin transfected migrating keratinocytes were quantified by bead displacements as described above whereas only single images were analyzed. Images were taken from time lapse acquisitions of two different cells. Minimum time interval between two images was 20 min. In total, 8 images were analyzed. To obtain a reference image without substrate deformation, cells were detached from the substrate by trypsination and a subsequent incubation in 20 mM NH_4OH to remove residual proteins. FAs were marked manually as the origin of force application. Forces were calculated as point forces for every FA as described before [Cesa et al., 2007]. Overall contraction forces of a cell were quantified as generalized first moment as defined in reference [Cesa et al., 2007]. To distinguish between nascent and mature

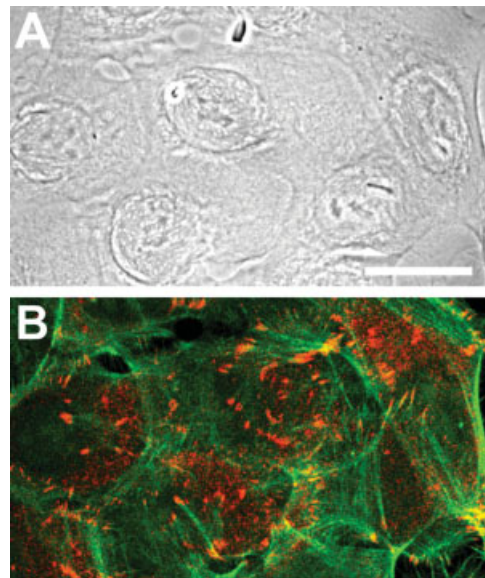


Fig. 1. Sessile keratinocytes. Keratinocytes were grown for 5 days. As a result, cells formed cell-cell contacts (A) and showed unpolarized, sessile behavior. Immunofluorescence staining against vinculin (red) and actin (green) (B) revealed roundish FAs coupled to actin stress fibers. Scale bar = $20 \mu\text{m}$.

FAs, a $14 \mu\text{m}$ wide region was defined for every analyzed image at the rear of the cell. FAs inside this region were referred to as matured FAs, all others as nascent FAs.

For FA size determination images of GFP transfected cells grown on PDMS were automatically segmented as described by microscopic techniques. For comparison, FAs of GFP-vinculin transfected cells grown on glass were analyzed identically. In total, 498 FAs on PDMS (eight independent images) and 2749 FAs on glass (25 independent images) were analyzed.

RESULTS

Cytoplasmic Diffusion Dominates Exchange Dynamic Analyses on Short Time Scales

Little is known about protein exchange dynamic processes during focal adhesion maturation. Since vinculin is one of the central proteins in the adhesion complex affected by several regulatory pathways on the level of activation, incorporation and phosphorylation [Bakolitsa et al., 2004; Chen et al., 2005], we used vinculin as model protein. In a first approach, vinculin exchange dynamics was analyzed in FAs of sessile keratinocytes. Sessile keratinocytes were typically unpolarized and adhered to neighboring cells (Figs. 1A and 1B). Their FAs displayed a roundish shape, were uniformly distributed over the entire cell and connected to actin stress fibers. FAs of sessile cells were stable in location and

intensity for hours. Despite the existence of lamellipodial dynamics, the formation of new adhesion structures was rarely detected (data not shown) indicating that all adhesions were mature and highly uniform.

To visualize protein exchange dynamics, sessile keratinocytes were transfected with GFP-vinculin. In fluorescence microscopy, FAs appeared as distinct bright spots indicating high concentration of bound vinculin, whereas a considerable fraction of vinculin remained present in the cytoplasm appearing as diffuse background within the cell (Fig. 2A). The rate and amount of vinculin exchange in FAs were measured using FRAP. Here, GFP-vinculin was photobleached at FAs and the mean fluorescence intensity I_{ad} at the bleached spot was recorded over time (Figs. 2A and 2B). We observed a fluorescence recovery in the bleach field due to replacement of bleached by unbleached proteins. The mean intensity I_{ref} of a reference adhesion outside the bleach field was recorded to determine unwanted bleaching due to image acquisition (Figs. 2A and 2B). The resulting recovery curves showed saturation values much lower than the initial (i.e. prebleach) intensity for the bleached areas I_{ad} . As the intensity I_{ref} at the reference adhesion site remained relatively stable over time, the decrease in intensity of I_{ad} was only partially due to unintended photobleaching during image acquisition (Fig. 2B). Instead, the data indicated a distinct pool of stably incorporated vinculin into FAs. A possible reason for partial recovery could have been the destruction of stably bound vinculin or other FA proteins presenting vinculin binding sites due to the high laser beam intensity during photobleaching. This was excluded by repeating the FRAP experiments at the same adhesion site which resulted in nearly identical recovery curves (Fig. S2).

Analyzing I_{ad} in more detail, a biphasic recovery was found (Fig. 2B). Similar vinculin recoveries had been observed previously [Lele et al., 2006; Humphries et al., 2007] and were interpreted as two independent binding/unbinding processes. As in our cells, freely diffusing vinculin caused a significant background, biphasic recovery could also be due to superposition of a slow exchange process and a fast diffusion of vinculin above the FA. This was experimentally verified by analyzing the fast recovery at FAs with regards to the size of the bleached area as described in the Supporting Information. Since these experiments revealed the cytoplasmic diffusion to be ~ 10 times faster than the slow binding process in FAs, we eliminated diffusion from all subsequent data by cutting the recovery curves at the visible kink (Fig. 2B, time t_k).

Based on the separation of cytoplasmic diffusion from vinculin exchange kinetics in FAs, recovery curves for stationary cells reached a mean saturation value of

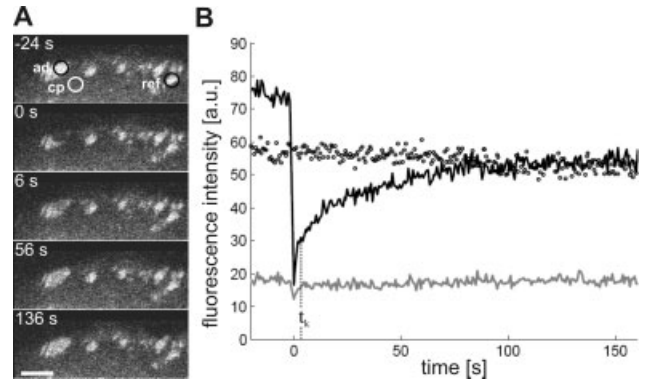


Fig. 2. Typical FRAP data. Sessile keratinocytes were transfected with GFP-vinculin and subsequently analyzed by FRAP. (A) Two bleach fields, one at a focal adhesion (ad) and one at a cytoplasmic site (cp) are given before (-24 s) directly after (0 s) and at three subsequent time points. A reference adhesion site (ref) was selected but not bleached to determine unintended photobleaching due to image acquisition. Radii of bleach fields were $1 \mu\text{m}$. Scale bar = $5 \mu\text{m}$. (B) Mean fluorescence intensities I of the bleach fields presented in A (I_{ad} : adhesion, black line; I_{cp} : cytoplasm, gray line) and the reference adhesion site (I_{ref} , circles) are given in arbitrary units (a.u.). I_{ad} shows a biphasic recovery with a visible kink at $t_k = 3.5$ s. Data were collected at a rate of one frame per second.

52% (SE = 2%, $n = 14$ FAs from 10 cells, blue curve, SE: σ/\sqrt{n}) with respect to the initial intensity (Fig. 3B and 3C). We were able to fit a single exponential model to our data describing a simple binding/unbinding process. The mean recovery half-time $t_{1/2}$ obtained by the fit was 57 s (SE = 5 s).

Vinculin Exchange Dynamics Attenuates in FAs During Maturation

FAs of migrating cells undergo a maturation process starting with their formation at the cell front and ending with their disassembly at the rear of the cell [Webb et al., 2002; Zaidel-Bar et al., 2004]. Since all present exchange analyses for FA proteins were performed on static cells at a distinct morphological state, we investigated whether such exchange dynamics could be regulated upon FA maturation. FRAP experiments were performed on nascent FAs at the front as well as on mature FAs at the rear of moving keratinocytes. Nascent FAs were located in the lamellipodium just behind the leading edge and were elongated in shape. They were connected to the loose lamellipodial actin meshwork consisting of small bundles mostly oriented parallel to the leading edge (Fig. 3A, inset). With an age of 6 to 15 minutes at first bleaching, all analyzed nascent FAs were relatively young but fully developed and stable in shape and fluorescence intensity. Mature FAs were located at the rear of cells and offered a roundish shape. Similar to FAs in stationary cells, they were predominantly associ-

ated with stress fibers (Fig. 3A, arrowheads). All examined matured FAs had an overall age of ~30 min and dissolved within 6 to 13 min after photobleaching in the course of rear release during migration. All experiments where FA disassembly occurred earlier, were rejected, since a stable plateau of the recovery curve was essential to determine a reliable saturation value.

In nascent FAs the mean recovery curves reached 70% (SE = 4%, $n = 14$ FAs from 9 cells) of its initial intensity. The recovery of mature adhesions in migrating cells was significantly lower, demonstrating a smaller fraction of constantly exchanging vinculin. It saturated at 49% (SE = 5%, $n = 11$ FAs from 11 cells), which was similar to the recovery of FAs in stationary cells. The mean recovery half-time in nascent FAs was 36 s (SE = 5 s) while in mature FAs the exchange rate was not significantly different (42 s, SE = 6 s) (Figs. 3B and 3C). In all cases vinculin exchange rates were significantly faster in motile than in sessile cells. These results demonstrate a decreasing exchange of vinculin in FAs over time reaching a maximum stabilization within FAs of sessile cells exhibiting the most persistent adhesion sites.

FAs With Stably Incorporated Vinculin Transmit Higher Traction Forces Than Nascent FAs

Vinculin is essential for mechano-coupling of FAs [Mierke et al., 2008]. Therefore, the results described above let us search for a connection between vinculin exchange and mechano-coupling of nascent and mature FAs. For this reason, we measured tractions of cells migrating on flexible silicone substrates coated with fibronectin by analyzing substrate deformation. The deformation was quantified by the displacement of fluorescent beads embedded in a top layer of the substrate. Repetitive microscopic analyses of PDMS substrates incubated with fluorescently labeled fibronectin proved to be a homogeneous substrate coating. Furthermore, substrate rigidity did not affect mean migration velocity of the

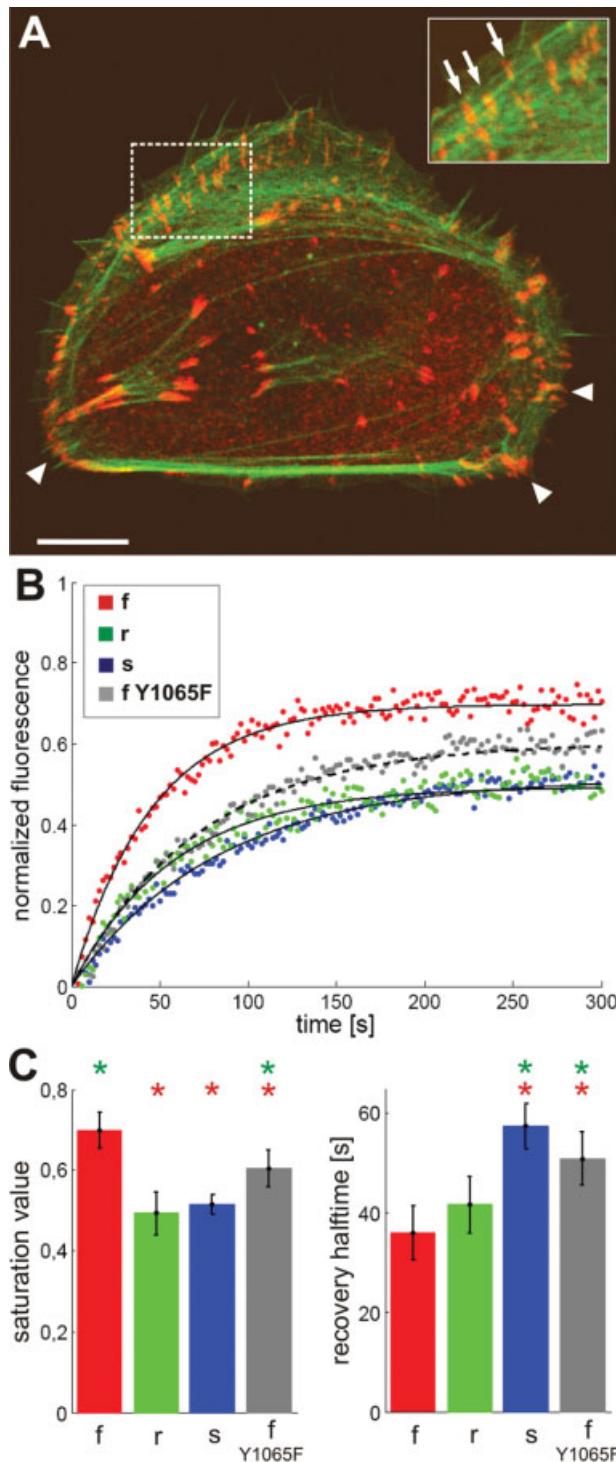


Fig. 3. Vinculin exchange dependence on the maturation state of FAs. (A) Fluorescent staining of a migrating keratinocyte for actin (green) and vinculin (red). Nascent adhesions develop in the lamella behind the leading edge and exhibit an elongated shape (inset, arrows). The lamella contains a loose actin meshwork consisting of small bundles that are mostly oriented parallel to the leading edge and perpendicular to focal adhesions (inset). Mature focal adhesions are mainly located at the back and are typically bigger than nascent adhesions (arrowheads). They are predominantly connected to strong actin bundles and dissolve in the course of rear release during the migration process. Scale bar = 10 μ m. (B) Mean fluorescence recovery of EGFP-vinculin in front (f) and rear (r) FAs of migrating cells and FAs of sessile cells (s) was analyzed. Additionally, mean fluorescence recovery of EGFP-vinculin Y1065F was measured in frontal FAs of migrating cells (f Y1065F). A single exponential model was fitted to the data (see Materials and Methods and Supporting Information) describing a simple binding/unbinding kinetics. (C) Mean saturation values and recovery half-times of all experimental curves that contributed to mean recovery curves depicted in B ($n = 14$ for f and s, $n = 11$ for r, $n = 13$ for f Y1065F). Asterisks designate a statistically significant difference from frontal (red) or rear (green) adhesions. The saturation value is significantly lower in mature FAs (r, s) compared to nascent FAs (f). For EGFP-vinculin Y1065F, the saturation value of nascent adhesions is diminished.

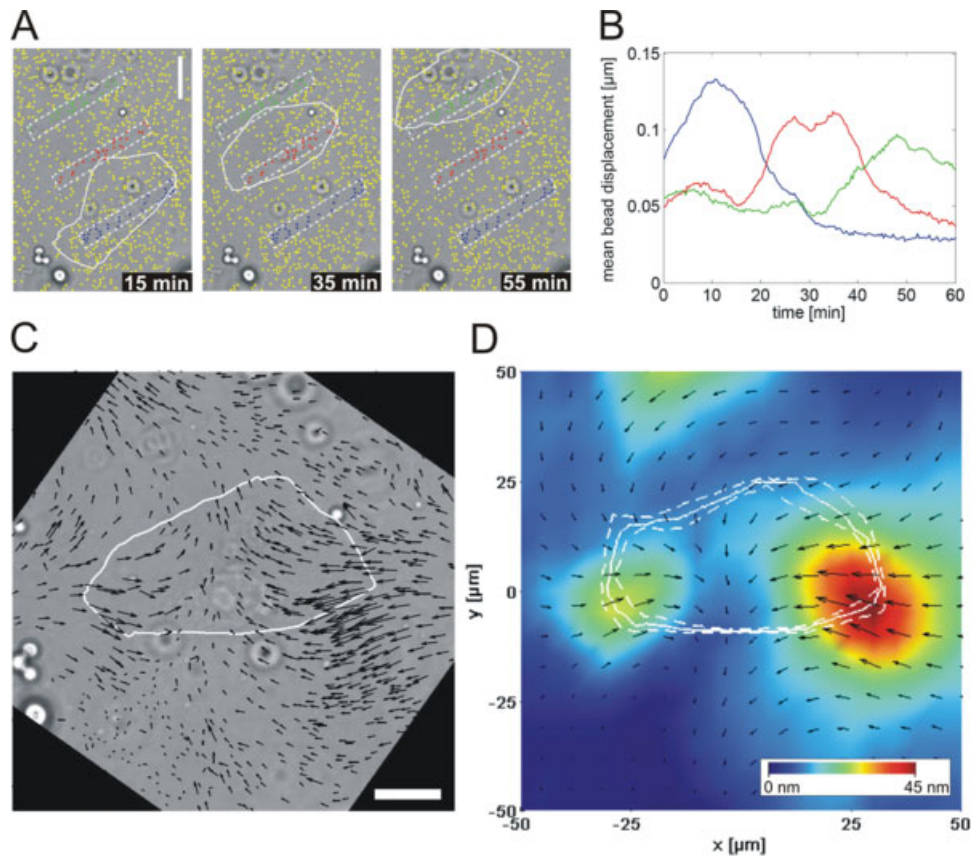


Fig. 4. Substrate bead displacement during migration. (A) Phase-contrast image sequence of a keratinocyte migrating over a PDMS-substrate. Due to reduced contrast, cell shape is indicated by a white line. The colored dots mark fluorescent beads embedded in the substrate localized to high accuracy with fluorescence microscopy. The blue, red and green labeled beads are located in three different regions of interest (white dashed borders) used for bead displacement analysis. Scale bar = 20 μm . (B) Mean bead displacement for the three regions of interest shown in A is given over time. (C) Phase-contrast image of the keratinocyte shown in A at 30 min. The cell shape is indicated by the white line. The nucleus was centered, and the image rotated resulting in an upward cell orientation. The arrows indicate the bead displacement magnified by a factor of 150. Scale bar = 15 μm . (D) Map

of mean bead displacements over 30 min. To fix the cell at the image center over the whole time series, each frame was shifted and rotated as shown in C. The mean cell shape (median) during the examined period is indicated by the solid white line and its statistical variance (0.25 and 0.75 quantile) is given by the dashed white lines. The black arrows show the mean bead displacement magnified by a factor of 200. Displacements are indicated in pseudo-colors. Note for D, that because of the short time span analyzed, the reference image (last image of time series) was still partially affected by the cellular deformation field. Mean bead displacements do, therefore, not sum up to zero. A is available in the Supporting Information as video 1. C is available as video 2.

cells with $\sim 1 \mu\text{m}/\text{min}$ for PDMS as well as glass substrates (data not shown). Moreover, mean size of FAs in GFP-vinculin transfected cells on the two different substrates was nearly the same (glass: $1.03 \mu\text{m}^2$, SE = $0.03 \mu\text{m}^2$, $n = 2749$; PDMS: $1.21 \mu\text{m}^2$, SE = $0.05 \mu\text{m}^2$, $n = 498$). Thus, migration and adhesion of keratinocytes was not affected by substrate rigidity.

In a first approach, the mean deformation was recorded for defined substrate areas over which the cell moved (Fig. 4A, Video 1). Substrate deformation increased while the cell crawled over it and decreased after the end of the cell had passed this area. The maximum substrate deformation was reached when the area of analysis was occupied by the rear end of the cell (Fig. 4B). Spatial distribution analysis of tractions at one time

point revealed most prominent deformations at the left and right of the rear cell end. Substrate deformations were directed inwards and perpendicular to the direction of migration (Fig. 4C). This result was confirmed by quantifying average bead displacements and cell shape over a time period of 30 min (Fig. 4D, Video 2). Displacements were concentrated at the rearmost corners of the cell, where mature adhesions with enhanced levels of stably incorporated vinculin are located (Fig. 3A; arrowheads). Mean displacements in the region of nascent adhesions in the lamellipodium were relatively weak and directed backwards.

In order to determine forces from substrate deformation patterns, keratinocytes were transfected with GFP-vinculin to visualize FAs and motility was induced.

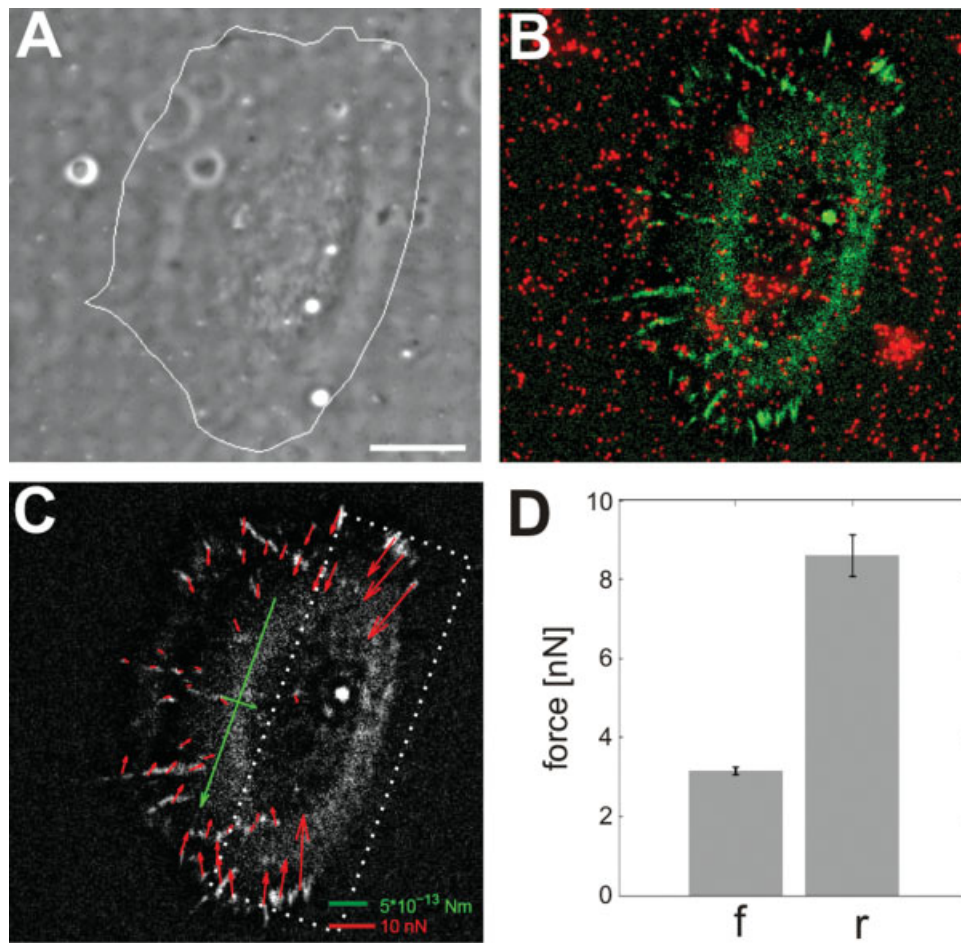


Fig. 5. Force application by motile cells. Keratinocytes were transfected with GFP-vinculin and cultured on micropatterned PDMS substrates. Cells were induced for migration and subsequently analyzed by video microscopy in phase contrast (A) and fluorescence microscopy in order to visualize FAs (green) and bead pattern (red) (B). Scale bar = 10 μ m. (C) Cell force calculation was performed for each FA. The eigenvectors of the generalized first moment tensor are indi-

cated by the green arrows. Applied forces for all analyzed nascent FAs (f, $n = 274$ FAs of eight images from 2 cells) and mature FAs (r, $n = 87$ FAs of eight images from 2 cells) are shown with error bars indicating standard error SE (D). To distinguish between nascent and mature FAs all adhesion sites in the rear 15 μ m of a cell were assumed to be mature [dashed box in (C)].

Cell force analyses on single images revealed a strong force concentration at the rear of the cell in the range of 8.6 nN per focal adhesion (SE = 0.54 nN, $n = 87$ FAs of eight images from two cells), where mature adhesions of stably incorporated vinculin were located. Elongated nascent adhesions applied much weaker forces of 1.7 nN (SE = 0.10 nN, $n = 274$ FAs of eight images from two cells) to the substrate (Fig. 5). These experiments reveal that the major traction forces are transmitted by mature adhesions during the whole migration process.

Vinculin Tyrosine Phosphorylation Decreases During FA Maturation

Our results suggest a modulation of force transduction and adhesion strength by regulated vinculin exchange dynamics. We, therefore, investigated on what

level vinculin exchange might be controlled. Recent studies revealed activation of vinculin during FA development by a conformational switch into an actin binding state [Chen et al., 2005]. As for other FA proteins, this activation is also believed to be regulated or stabilized by phosphorylation at distinct tyrosine residues [Johnson and Craig, 1994; Zhang et al., 2004].

To determine the amount of vinculin phosphorylation, we measured the ratio of total to tyrosine-phosphorylated vinculin for individual FAs by quantitative immunostaining assays. These studies revealed a barely detectable vinculin phosphorylation level for fully matured FAs of stationary cells (Fig. 6). A significantly higher vinculin phosphorylation level was found in motile keratinocytes. Here, especially nascent FAs at the lamellipodial front were highly phosphorylated and,

therefore are in good agreement to earlier data [Zamir et al., 1999]. To separate nascent from mature FAs in migrating cells, we analyzed their phosphorylation ratio with respect to their distance from the leading edge (Fig. 6B). This distance was used as a measure for maturation state of FAs. Within 0 to 5.5 μm distance from the leading edge, vinculin phosphorylation was significantly higher compared to stationary cells and decreased uniformly towards the rear of the cell. All nascent FAs with increased vinculin exchange identified by us were located in the same cell region (1.7 to 5.4 μm from the leading edge at bleach time). Beyond 5.5 μm distance

from the leading edge, vinculin-phosphorylation remained stable at a low level and no significant difference could be detected compared to stationary cells. These data point to a regulation of vinculin exchange dynamics by vinculin phosphorylation.

Vinculin Exchange Dynamics is Directly Coupled to Phosphorylation at Tyrosine 1065

To identify the responsible regulatory pathway, a mutated GFP-vinculin Y1065F version was generated to inhibit tyrosine 1065 phosphorylation by c-src kinase and to affect vinculin activation [Zhang et al., 2004; Moese et al., 2007]. Performing FRAP experiments with GFP-vinculin Y1065F on young FAs revealed mean saturation values of 60% (SE = 5%, $n = 13$ FAs from nine cells, grey curve in Fig. 3B) and recovery half times of 51 s (SE = 5 s) (Figs. 3B and 3C). Although experimental conditions were kept identical to those described above for nonmutated GFP-vinculin in young FAs, mutating just a single tyrosine at position 1065 resulted in a strong reduction of exchange dynamic regulations during maturation of FAs. Mean saturation values as well as $t_{1/2}$ of vinculin Y1065F in nascent FAs were significantly lower demonstrating that exchange dynamics of vinculin is regulated by phosphorylation at the single tyrosine residue Y1065.

DISCUSSION

Cellular adhesions undergo extensive changes in protein composition during their life cycle. At the same time protein modification, especially tyrosine phosphorylation, takes place. Exchange of proteins is an important step in FA remodeling because any type of regulation or modification must at least partially alter the on/off rates for FA protein interaction to allow FA dynamics and remodeling. Dynamic processes have been observed

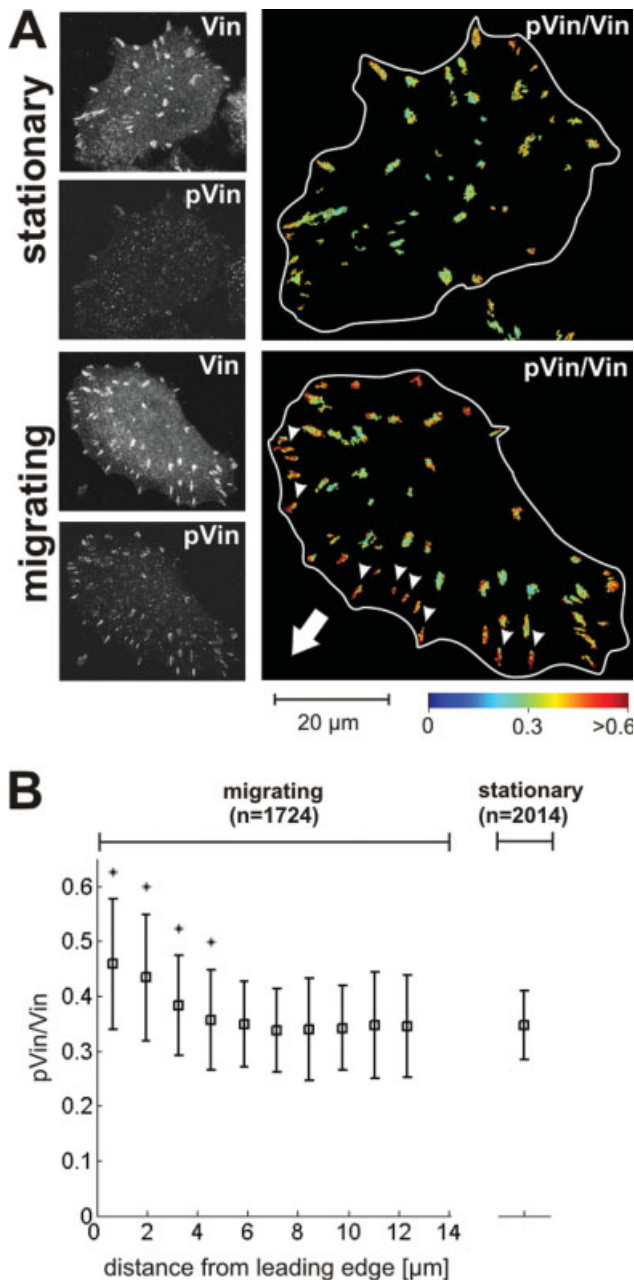


Fig. 6. Phosphorylation levels of vinculin in FAs (A) Immunostaining of stationary and migrating keratinocytes against vinculin (Vin) and phosphorylated vinculin (pVin). Images on the right present the ratio between phosphorylated and total vinculin within FAs in a pseudo color scale. Note, that the high phosphorylation of nascent FAs at the leading edge of the migrating cell (arrowheads). Ratios are given for each pixel separately. Automated identification of FAs was performed as described earlier (Zamir et al., 1999). Cell shapes are indicated by solid white lines. The big white arrow shows the direction of migration. (B) Mean vinculin phosphorylation (pVin/Vin) of FAs in migrating cells with respect to their distance from the leading edge (left) and in stationary cells (right). In migrating cells, vinculin phosphorylation in FAs decreases with increasing distance to the leading edge. Asterisks indicate significant differences of vinculin phosphorylation compared to FAs of stationary cells given on the right. Error bars indicate standard deviation. $n =$ number of analyzed FAs of 38 migrating and 21 sessile cells.

on almost any time scale from focal complex formation upon cell spreading [Zimmerman et al., 2004] or FA size adaptation [Riveline et al., 2001] to external stress application and long term FA alterations, e.g. during cell differentiation [Hinz and Gabbiani, 2003; Hinz et al., 2004]. In all of these examples, the described processes go along with changes in protein composition and/or modified tyrosine phosphorylation patterns [Bershadsky et al., 2003]. Postulations of protein activation by tyrosine phosphorylation could be proven for several proteins such as vinculin [Goldmann et al., 1998; Zhang et al., 2004], paxillin [Zaidel-Bar et al., 2007b] or FAK [Schaller et al., 1994; Calalb et al., 1996; Hamadi et al., 2005] which provide a rationale for the observed high levels of phosphotyrosine in nascent FAs. Yet, little was known on how regulatory events affect exchange kinetics of FA proteins and recovery halftimes or mean saturation values in FRAP experiments. Former studies revealed a connection between tyrosine phosphatase 2 activity and exchange kinetics of FA proteins [von Wichert et al., 2003]. Due to these findings it was speculated that phosphorylation regulates FA maturation by altering protein exchange dynamics as a mechanism to control adhesion strength [Ziegler et al., 2006]. Our experiments support this theory by proving strongly regulated protein exchange dynamics during FA maturation and dependencies of exchange dynamics regulations on protein phosphorylation and adhesion strength. Beyond these general principles, regulation of vinculin exchange dynamics could be directly linked to phosphorylation at tyrosine 1065. Inhibition of just one single phosphorylation site resulted for young FAs in a significantly reduced exchanging fraction and exchange rate of vinculin. Since mature FAs are characterized by only a low vinculin phosphorylation level, phosphorylation at Y1065 seems to play a major role in regulating vinculin exchange dynamics and FA maturation. More precisely, we propose that the growth dynamics of FAs as well as their ability to transduce mechanical forces are at least partially controlled by a direct modulation of vinculin exchange dynamics (Fig 7). According to our model, enhancing vinculin exchange by phosphorylation leads to a mechanical destabilization of the whole adhesion complex and enables the complex to grow as it is particularly pronounced in nascent adhesions. During maturation, these complexes become stabilized by vinculin dephosphorylation leading to a mechanically resistant adhesion with constant shape. Various studies show the essential role of vinculin for force transduction [Gallant et al., 2005; Mierke et al., 2008]. Moreover, the claim that phosphorylation enables individual FAs to adapt in size is supported by the finding, that mature FAs, which are normally unphosphorylated, lack the ability to grow upon external force application [Galbraith et al., 2002].

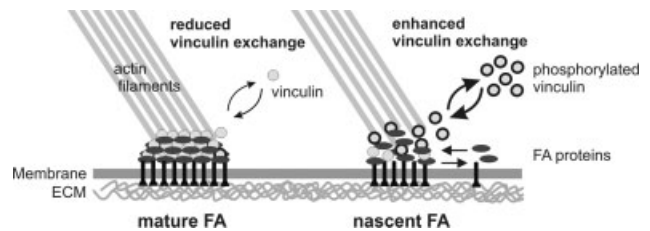


Fig. 7. Model for vinculin exchange dependent adhesion maturation. In nascent FAs (right) mainly phosphorylated vinculin is present and bound with high exchange dynamics within the complex. This enhanced dynamics allows incorporation of new FA proteins and therefore size adaptations of nascent FAs but at the same time it diminishes the ability to transduce strong traction forces. In contrast, mature FAs (left) are very stable structures able to resist strong tractions. Here, most of the vinculin molecules are dephosphorylated and firmly embedded in the adhesion complex.

Thus, our data support the theory that tyrosine phosphorylation enhances exchange dynamics in order to form or adapt FAs within short time scales while tyrosine dephosphorylation is a prerequisite for FA maturation and stable FA over time. Nevertheless, it is very likely, that phosphorylation at tyrosine 1065 is not the only site to regulate vinculin dynamics. Although significantly lowered, the exchanging fraction of phosphorylation-inhibited vinculin in nascent FAs was still above the value found in mature FAs.

In the past, FRAP analyses on various stationary cell types revealed widely scattered halftimes as well as saturation values. Analyses on 3T3 cells and BALB/c fibroblasts showed recovery halftimes in the range of 5 min and mean saturation values of 90% for α -actinin [Edlund et al., 2001]. Other experiments reported recovery halftimes in the range of 45 s in rat embryonic fibroblasts and 30 s in glioblastoma cells for the same protein [Fraleley et al., 2005] and values of 14 s and 1 min, respectively, for endothelial cells [Tsuruta et al., 2002; Lele et al., 2008]. Similar differences in recovery halftimes were observed for other FA proteins such as β 3-integrin [Tsuruta et al., 2002; Lele et al., 2008], paxillin [von Wichert et al., 2003; Cohen et al., 2006], talin [Gupton and Waterman-Storer, 2006; Lele et al., 2008] or vinculin [von Wichert et al., 2003; Cohen et al., 2006]. These variations were mainly explained by different protein binding partners in different cell types [Lele et al., 2008]. Further to that we want to discuss two additional possibilities for the differences in protein exchange dynamics. The first one relates to very short recovery halftimes, while the second concerns the broad exchange dynamics distribution. In very dynamic cell types such as keratinocytes, recovery curves can be strongly affected by cytoplasmic diffusion of high levels of expressed GFP-fusion proteins. This can lead to a pronounced biphasic recovery curve [Lele et al., 2004]. While in

other publications biphasic recovery curves were due to two independent binding/unbinding processes [Lele et al., 2006], in our system vinculin's first phase recoveries were mainly caused by diffusion. The main argument for this conclusion is the strong dependence of initial recovery kinetics on bleach field widths shown in Fig. S3.

While there is a possibility that the diffusion process is superimposed by an additional fast vinculin binding event which might contribute to the initial recovery, a diffusion constant for cytoplasmic GFP-vinculin of $1.5 \mu\text{m}^2/\text{s}$ is reasonable and argues for a dominant contribution of recovery in the subsecond regime for bleach field areas as used for FRAP experiments on FAs (in our case on average $10 \mu\text{m}^2$). Comparing our GFP-vinculin diffusion constant with diffusion coefficients of other cytoplasmic proteins of similar size (e.g. GFP-androgen receptor) [Farla et al., 2005], vinculin seems to diffuse just slightly slower. Therefore, our findings illustrate the importance of diffusion for the determination of reliable protein exchange kinetics and supports the results of earlier theoretical studies [Lele et al., 2004].

The second point to explain current half-time variations is the direct regulation of recovery halftimes and saturation values during FA maturation identified here. Recent findings argue for a putative dependence between ligand binding or protein phosphorylation and FA protein recovery. For α -actinin, binding to phosphoinositides enhances protein recovery in stress fibers as well as FAs [Fraleigh et al., 2005]. FAK phosphorylation at tyr397 has also been shown to increase recovery halftimes in FAs [von Wichert et al., 2003]. Since ligand binding, protein composition and phosphorylation pattern change with FA maturation, it is very likely that recovery halftimes of FA proteins are hardly comparable between distinct cell types. This hypothesis is strengthened by our FRAP experiments on sessile as well as motile keratinocytes. Here, FAs of sessile cells with their fully matured adhesion structures are characterized by vinculin recovery halftimes as well as mean saturation values similar to those of stationary human foreskin fibroblasts [Cohen et al., 2006]. In contrast, nascent FAs of the identical cell type show much faster vinculin recoveries with higher fractions of exchanging protein. With time and further FA maturation, the same FAs are regulated by their protein exchange dynamics in direction of sessile cells.

Based on our repetitive bleaching experiments on sessile cells, we could additionally show that exchanging and stably incorporated vinculin fractions do not interact on the time scale of our measurements. This conversion would lead to nonoverlapping bleach curves which are not found in our experiments. We estimate that the persistence time of stably incorporated vinculin would

exceed 30 min since lower persistence times would have resulted in measurable effects.

One can only speculate if GFP as bulky label might affect the exchange dynamics of vinculin. In our experiments, these effects should be negligible because cell adhesion and FA dynamics are unaffected. Only cytoplasmic diffusion and therefore on/off rates of larger fusion constructs might be affected. However, since our data reveal diffusion to take place at much shorter time scales than vinculin exchange kinetics, this effect should be negligible as well.

Exchange kinetics can be additionally affected by the effective cytoplasmic protein concentration (c_c). In our case this concentration is on average increased by a factor of 3 to 5 in cells expressing GFP-vinculin versions (see Supporting Information, Fig. S4). However, we have always chosen cells expressing very low levels of GFP-vinculin for our FRAP analyses arguing that c_c was even less affected. Furthermore, control FRAP analyses on sessile cells expressing very high levels of GFP-vinculin resulted in comparable recovery halftimes and mean saturation values (data not shown). These data additionally imply that vinculin exchange kinetics is mainly regulated at the level of the unbinding rate k_{off} .

Our cell force measurements on moving keratinocytes reveal enhanced force generation at the rear corners while nascent lamellipodial adhesions apply much weaker forces per FA. These findings are consistent with earlier experiments carried out on migrating fish keratinocytes [Oliver et al., 1999]. These cells also revealed strong inwards directed forces at both rear sites indicating "pincer-like tractions" while the lamellipodial tractions were very low. As confirmed by numerical simulations, the method we used for calculating force measurements resolves traction forces within a distance of $\sim 2 \mu\text{m}$ [Schwarz et al., 2002]. With such a high spatial resolution it was possible to differentiate between forces of nascent and mature FAs, which were usually more than $10 \mu\text{m}$ away from each other (Fig. 3A). Interestingly, force measurements on goldfish fibroblasts revealed contrary results with small nascent adhesions that applied strong traction forces [Beningo et al., 2001]. At this point the reason for this difference remains open. A lower phosphorylation level in nascent FAs of fish fibroblasts or a very fast dephosphorylation and therefore early maturation and stabilization of these FAs appears possible. Since fibroblasts describe a less dynamic cell type compared to fast regulatory processes of keratinocytes, the level of phosphorylation might also be less important in those cells.

In summary, our data show the down-regulation of vinculin exchange dynamics during FA maturation. This maturation process goes along with a decrease of vinculin phosphorylation level and increasing adhesion

strength. Moreover, inhibition of vinculin phosphorylation by a single point mutation at Y1065 diminishes vinculin exchange dynamics in nascent FAs. The data, therefore, support on the molecular level former models proposing a regulation of adhesion strength by modifying vinculin exchange dynamics and phosphorylation levels [Zamir et al., 1999; Zhang et al., 2004; Ziegler et al., 2006; Zaidel-Bar et al., 2007b].

ACKNOWLEDGMENTS

The authors thank D. Kirchenb uchler, O. D. Gordan, and U. Zedler for helpful discussions and critical reading of the manuscript. The GFP-vinculin construct was kindly provided by B. Geiger (Weizmann Institute of Science, Israel).

REFERENCES

- Anderson KI, Cross R. 2000. Contact dynamics during keratocyte motility. *Curr Biol* 10(5):253–260.
- Bakolitsa C, Cohen DM, Bankston LA, Bobkov AA, Cadwell GW, Jennings L, Critchley DR, Craig SW, Liddington RC. 2004. Structural basis for vinculin activation at sites of cell adhesion. *Nature* 430(6999):583–586.
- Balaban NQ, Schwarz US, Riveline D, Goichberg P, Tzur G, Sabanay I, Mahalu D, Safran S, Bershadsky A, Addadi L, Geiger B. 2001. Force and focal adhesion assembly: a close relationship studied using elastic micropatterned substrates. *Nat Cell Biol* 3(5):466–472.
- Beningo KA, Dembo M, Kaverina I, Small JV, Wang YL. 2001. Nascent focal adhesions are responsible for the generation of strong propulsive forces in migrating fibroblasts. *J Cell Biol* 153(4):881–888.
- Bershadsky AD, Balaban NQ, Geiger B. 2003. Adhesion-dependent cell mechanosensitivity. *Annu Rev Cell Dev Biol* 19:677–695.
- Calalb MB, Zhang X, Polte TR, Hanks SK. 1996. Focal adhesion kinase tyrosine-861 is a major site of phosphorylation by Src. *Biochem Biophys Res Commun* 228(3):662–668.
- Cesa CM, Kirchgessner N, Mayer D, Schwarz US, Hoffmann B, Merkel R. 2007. Micropatterned silicone elastomer substrates for high resolution analysis of cellular force patterns. *Rev Sci Instrum* 78(3):034301.
- Chen H, Cohen DM, Choudhury DM, Kioka N, Craig SW. 2005. Spatial distribution and functional significance of activated vinculin in living cells. *J Cell Biol* 169(3):459–470.
- Chrzanowska-Wodnicka M, Burridge K. 1996. Rho-stimulated contractility drives the formation of stress fibers and focal adhesions. *J Cell Biol* 133(6):1403–1415.
- Cohen DM, Kutscher B, Chen H, Murphy DB, Craig SW. 2006. A conformational switch in vinculin drives formation and dynamics of a talin-vinculin complex at focal adhesions. *J Biol Chem* 281(23):16006–16015.
- Edlund M, Lotano MA, Otey CA. 2001. Dynamics of alpha-actinin in focal adhesions and stress fibers visualized with alpha-actinin-green fluorescent protein. *Cell Motil Cytoskeleton* 48(3):190–200.
- Farla P, Hersmus R, Trapman J, Houtsmuller AB. 2005. Antiandrogens prevent stable DNA-binding of the androgen receptor. *J Cell Sci* 118 (Part 18):4187–4198.
- Fralely TS, Pereira CB, Tran TC, Singleton C, Greenwood JA. 2005. Phosphoinositide binding regulates alpha-actinin dynamics: mechanism for modulating cytoskeletal remodeling. *J Biol Chem* 280(15):15479–15482.
- Galbraith CG, Sheetz MP. 1997. A micromachined device provides a new bend on fibroblast traction forces. *Proc Natl Acad Sci USA* 94(17):9114–9118.
- Galbraith CG, Yamada KM, Sheetz MP. 2002. The relationship between force and focal complex development. *J Cell Biol* 159(4):695–705.
- Gallant ND, Michael KE, Garcia AJ. 2005. Cell adhesion strengthening: contributions of adhesive area, integrin binding, and focal adhesion assembly. *Mol Biol Cell* 16(9):4329–4340.
- Geiger B, Bershadsky A. 2002. Exploring the neighborhood: adhesion-coupled cell mechanosensors. *Cell* 110(2):139–142.
- Gilmore AP, Burridge K. 1996. Regulation of vinculin binding to talin and actin by phosphatidylinositol-4-5-bisphosphate. *Nature* 381(6582):531–535.
- Goldmann WH, Galneder R, Ludwig M, Xu W, Adamson ED, Wang N, Ezzell RM. 1998. Differences in elasticity of vinculin-deficient F9 cells measured by magnetometry and atomic force microscopy. *Exp Cell Res* 239(2):235–242.
- Grinnell F, Zhu M, Carlson MA, Abrams JM. 1999. Release of mechanical tension triggers apoptosis of human fibroblasts in a model of regressing granulation tissue. *Exp Cell Res* 248(2):608–619.
- Gupton SL, Waterman-Storer CM. 2006. Spatiotemporal feedback between actomyosin and focal-adhesion systems optimizes rapid cell migration. *Cell* 125(7):1361–1374.
- Hamadi A, Bouali M, Dontenwill M, Stoeckel H, Takeda K, Ronde P. 2005. Regulation of focal adhesion dynamics and disassembly by phosphorylation of FAK at tyrosine 397. *J Cell Sci* 118 (Part 19):4415–4425.
- Hinz B, Gabbiani G. 2003. Mechanisms of force generation and transmission by myofibroblasts. *Curr Opin Biotechnol* 14(5):538–546.
- Hinz B, Pittet P, Smith-Clerc J, Chaponnier C, Meister JJ. 2004. Myofibroblast development is characterized by specific cell-cell adherens junctions. *Mol Biol Cell* 15(9):4310–4320.
- Humphries JD, Wang P, Streuli C, Geiger B, Humphries MJ, Ballestrem C. 2007. Vinculin controls focal adhesion formation by direct interactions with talin and actin. *J Cell Biol* 179(5):1043–1057.
- Johnson RP, Craig SW. 1994. An intramolecular association between the head and tail domains of vinculin modulates talin binding. *J Biol Chem* 269(17):12611–12619.
- Johnson RP, Craig SW. 1995. The carboxy-terminal tail domain of vinculin contains a cryptic binding site for acidic phospholipids. *Biochem Biophys Res Commun* 210(1):159–164.
- Kesel AB, Junge MM, Nachtigall W. 1999. *Einführung in die angewandte Statistik für Biowissenschaftler*. Basel: Birkhäuser Verlag.
- Kirfel G, Rigort A, Borm B, Herzog V. 2004. Cell migration: mechanisms of rear detachment and the formation of migration tracks. *Eur J Cell Biol* 83(11–12):717–724.
- Lauffenburger DA, Horwitz AF. 1996. Cell migration: a physically integrated molecular process. *Cell* 84(3):359–369.
- Lele T, Oh P, Nickerson JA, Ingber DE. 2004. An improved mathematical approach for determination of molecular kinetics in living cells with FRAP. *Mech Chem Biosyst* 1(3):181–190.
- Lele TP, Pendse J, Kumar S, Salanga M, Karavitis J, Ingber DE. 2006. Mechanical forces alter zyxin unbinding kinetics within focal adhesions of living cells. *J Cell Physiol* 207(1):187–194.
- Lele TP, Thodeti CK, Pendse J, Ingber DE. 2008. Investigating complexity of protein-protein interactions in focal adhesions. *Biochem Biophys Res Commun* 369(3):929–934.

- Merkel R, Kirchgessner N, Cesa CM, Hoffmann B. 2007. Cell force microscopy on elastic layers of finite thickness. *Biophys J* 93(9):3314–3323.
- Mierke CT, Kollmannsberger P, Zitterbart DP, Smith J, Fabry B, Goldmann WH. 2008. Mechano-coupling and regulation of contractility by the vinculin tail domain. *Biophys J* 94(2):661–670.
- Moese S, Selbach M, Brinkmann V, Karlas A, Haimovich B, Backert S, Meyer TF. 2007. The *Helicobacter pylori* CagA protein disrupts matrix adhesion of gastric epithelial cells by dephosphorylation of vinculin. *Cell Microbiol* 9(5):1148–1161.
- Oliver T, Dembo M, Jacobson K. 1999. Separation of propulsive and adhesive traction stresses in locomoting keratocytes. *J Cell Biol* 145(3):589–604.
- Petit V, Thiery JP. 2000. Focal adhesions: structure and dynamics. *Biol Cell* 92(7):477–494.
- Riveline D, Zamir E, Balaban NQ, Schwarz US, Ishizaki T, Narumiya S, Kam Z, Geiger B, Bershadsky AD. 2001. Focal contacts as mechanosensors: externally applied local mechanical force induces growth of focal contacts by an mDia1-dependent and ROCK-independent mechanism. *J Cell Biol* 153(6):1175–1186.
- Rottner K, Hall A, Small JV. 1999. Interplay between Rac and Rho in the control of substrate contact dynamics. *Curr Biol* 9(12):640–648.
- Schaller MD, Hildebrand JD, Shannon JD, Fox JW, Vines RR, Parsons JT. 1994. Autophosphorylation of the focal adhesion kinase, pp125FAK, directs SH2-dependent binding of pp60src. *Mol Cell Biol* 14(3):1680–1688.
- Schwarz US, Balaban NQ, Riveline D, Bershadsky A, Geiger B, Safran SA. 2002. Calculation of forces at focal adhesions from elastic substrate data: the effect of localized force and the need for regularization. *Biophys J* 83(3):1380–1394.
- Small JV. 1981. Organization of actin in the leading edge of cultured cells: influence of osmium tetroxide and dehydration on the ultrastructure of actin meshworks. *J Cell Biol* 91(3 Part 1):695–705.
- Subauste MC, Pertz O, Adamson ED, Turner CE, Junger S, Hahn KM. 2004. Vinculin modulation of paxillin-FAK interactions regulates ERK to control survival and motility. *J Cell Biol* 165(3):371–381.
- Thomas JW, Cooley MA, Broome JM, Salgia R, Griffin JD, Lombardo CR, Schaller MD. 1999. The role of focal adhesion kinase binding in the regulation of tyrosine phosphorylation of paxillin. *J Biol Chem* 274(51):36684–36692.
- Tsuruta D, Gonzales M, Hopkinson SB, Otey C, Khuon S, Goldman RD, Jones JC. 2002. Microfilament-dependent movement of the beta3 integrin subunit within focal contacts of endothelial cells. *FASEB J* 16(8):866–868.
- Vogel V, Sheetz M. 2006. Local force and geometry sensing regulate cell functions. *Nat Rev Mol Cell Biol* 7(4):265–275.
- Volberg T, Geiger B, Citi S, Bershadsky AD. 1994. Effect of protein kinase inhibitor H-7 on the contractility, integrity, and membrane anchorage of the microfilament system. *Cell Motil Cytoskeleton* 29(4):321–338.
- von Wichert G, Haimovich B, Feng GS, Sheetz MP. 2003. Force-dependent integrin-cytoskeleton linkage formation requires downregulation of focal complex dynamics by Shp2. *EMBO J* 22(19):5023–5035.
- Wang HB, Dembo M, Wang YL. 2000. Substrate flexibility regulates growth and apoptosis of normal but not transformed cells. *Am J Physiol Cell Physiol* 279(5):C1345–C1350.
- Webb DJ, Parsons JT, Horwitz AF. 2002. Adhesion assembly, disassembly and turnover in migrating cells—over and over and over again. *Nat Cell Biol* 4(4):E97–E100.
- Zaidel-Bar R, Ballestrem C, Kam Z, Geiger B. 2003. Early molecular events in the assembly of matrix adhesions at the leading edge of migrating cells. *J Cell Sci* 116 (Part 22):4605–4613.
- Zaidel-Bar R, Cohen M, Addadi L, Geiger B. 2004. Hierarchical assembly of cell-matrix adhesion complexes. *Biochem Soc Trans* 32 (Part 3):416–420.
- Zaidel-Bar R, Itzkovitz S, Ma'ayan A, Iyengar R, Geiger B. 2007a. Functional atlas of the integrin adhesome. *Nat Cell Biol* 9(8):858–867.
- Zaidel-Bar R, Milo R, Kam Z, Geiger B. 2007b. A paxillin tyrosine phosphorylation switch regulates the assembly and form of cell-matrix adhesions. *J Cell Sci* 120 (Part 1):137–148.
- Zamir E, Geiger B. 2001. Molecular complexity and dynamics of cell-matrix adhesions. *J Cell Sci* 114 (Part 20):3583–3590.
- Zamir E, Katz BZ, Aota S, Yamada KM, Geiger B, Kam Z. 1999. Molecular diversity of cell-matrix adhesions. *J Cell Sci* 112 (Part 11):1655–1669.
- Zhang Z, Izaguirre G, Lin SY, Lee HY, Schaefer E, Haimovich B. 2004. The phosphorylation of vinculin on tyrosine residues 100 and 1065, mediated by SRC kinases, affects cell spreading. *Mol Biol Cell* 15(9):4234–4247.
- Ziegler WH, Liddington RC, Critchley DR. 2006. The structure and regulation of vinculin. *Trends Cell Biol* 16(9):453–460.
- Zimmerman B, Volberg T, Geiger B. 2004. Early molecular events in the assembly of the focal adhesion-stress fiber complex during fibroblast spreading. *Cell Motil Cytoskeleton* 58(3):143–159.